genitors do not require a gradient and will spread to cover an entire region of cells expressing *bnl* at equivalent levels. When *bnl*-expressing clones failed to induce migration, the clones appeared to be too far from the progenitors or there was competition from another clone close by (fig. S8, A and B). Ectopic *bnl* expression within the progenitor cluster arrested migration (fig. S8C).

The results show that the embryonic tracheal inducer Bnl FGF guides tracheal progenitors out of the niche and into the posterior during tracheal metamorphosis. The source of Bnl is the larval tracheal branches destined for destruction, which serve both as the source of the chemoattractant and as the substratum for progenitor migration. Several days earlier in embryos, these larval tracheal branches were themselves induced by Bnl provided by neighboring tissues. But after embryonic development, most tracheal cells, including those in the decaying larval branches, downregulate *btl* FGFR expression (fig. S2A) and thus do not respond to (or sequester) the Bnl signal they later express. One of the most notable aspects of this larval Bnl is its exquisitely specific pattern in decaying larval branches, which presages progenitor outgrowth. It is unclear how Bnl expression is controlled, though it does not appear to require signals from migrating progenitors because the *bnl* reporter expression front progressed normally when progenitor outgrowth was stalled by a tracheal break (fig. S6C). Perhaps expression of Bnl involves gradients in the tracheal system or spatial patterning cues established during embry-

Mutational Analysis Reveals the Origin and Therapy-Driven Evolution of Recurrent Glioma

Brett E. Johnson,[1]* Tali Mazor,[1]* Chibo Hong,[1] Michael Barnes,[2] Koki Aihara,[3,4] Cory Y. McLean,[1]† Shaun D. Fouse,[1] Shogo Yamamoto,[3] Hiroki Ueda,[3] Kenji Tatsuno,[3] Saurabh Asthana,[5,6] Llewellyn E. Jalbert,[7] Sarah J. Nelson,[7,8] Andrew W. Bollen,[2] W. Clay Gustafson,[9] Elise Charron,[10] William A. Weiss,[1,9,10] Ivan V. Smirnov,[1] Jun S. Song,[11,12] Adam B. Olshen,[6,11] Soonmee Cha,[1] Yongjun Zhao,[13] Richard A. Moore,[13] Andrew J. Mungall,[13] Steven J. M. Jones,[13] Martin Hirst,[13] Marco A. Marra,[13] Nobuhito Saito,[4] Hiroyuki Aburatani,[3] Akitake Mukasa,[4] Mitchel S. Berger,[1] Susan M. Chang,[1] Barry S. Taylor,[5,6,11]‡ Joseph F. Costello[1]‡

Tumor recurrence is a leading cause of cancer mortality. Therapies for recurrent disease may fail, at least in part, because the genomic alterations driving the growth of recurrences are distinct from those in the initial tumor. To explore this hypothesis, we sequenced the exomes of 23 initial low-grade gliomas and recurrent tumors resected from the same patients. In 43% of cases, at least half of the mutations in the initial tumor were undetected at recurrence, including driver mutations in *TP53*, *ATRX*, *SMARCA4*, and *BRAF*; this suggests that recurrent tumors are often seeded by cells derived from the initial tumor at a very early stage of their evolution. Notably, tumors from 6 of 10 patients treated with the chemotherapeutic drug temozolomide (TMZ) followed an alternative evolutionary path to high-grade glioma. At recurrence, these tumors were hypermutated and harbored driver mutations in the RB (retinoblastoma) and Akt-mTOR (mammalian target of rapamycin) pathways that bore the signature of TMZ-induced mutagenesis.

The genetic landscape of tumors is continually evolving, which can be an impediment to the clinical management of cancer patients with recurrent disease (*1*, *2*). In contrast to the clonal evolution of hematological malignancies (*3*, *4*) and solid tumor metastases (*5*–*7*), the local regrowth of solid tumors after surgery occurs under a unique set of evolutionary pressures, which are further affected by adjuvant therapies. Through the acquisition of new mutations, residual tumor cells can progress to a more aggressive state. Grade II astrocytic gliomas are

particularly troublesome from this perspective. Although surgery is the standard of care, these invasive brain tumors typically recur (*8*). Many remain grade II at recurrence, while others progress to a higher histological grade with a poor prognosis (*9*). The incidence and timing of malignant progression are variable and unpredictable (*8*).

We undertook genome sequence analysis of initial and recurrent human gliomas to address two questions: (i) What is the extent to which mutations in initial tumors differ from their subsequent recurrent tumors? (ii) How does chemotherapy with temozolomide (TMZ), a drug commonly used in the treatment of glioma, affect the mutational profile of recurrent tumors? We sequenced the exomes of 23 grade II gliomas at initial diagnosis and their recurrences resected from the same patients up to 11 years later (table S1). We selected initial tumors of predominantly astrocytic histology that capture the full spectrum of glioma progression (histological grade II to IV at recurrence) and adjuvant treatment history. Tumor and matched normal DNA were sequenced to an average 125-fold coverage, enabling the sensitive detection of mutations down to a 10% variant frequency, small insertions and deletions, and DNA copy number alterations (CNAs) (Fig. 1A and tables S2 and S3) (*10*).

We identified an average of 33 somatic coding mutations in each initial tumor, of which an average of 54% were also detected at recurrence (shared mutations) (Fig. 1A). The shared mutations included those in *IDH1*, *TP53*, and *ATRX* in most but not all cases (fig. S1) (*11*–*13*). All other somatic mutations were identified only in the initial tumor or only in the recurrent tumor from a given patient (private mutations) and thus presumably arose later in tumor evolution. For example, mutations in *SMARCA4* were private to the initial or recurrent tumor in six of seven patients and therefore may confer a selective advantage in the context of preexisting early driver events (*14*, *15*). Overall, the initial and recurrent gliomas displayed a broad spectrum of genetic relatedness (fig. S2 and table S4). At one end of this spectrum were four patients whose tumors showed a pattern of linear clonal evolution; we infer that the recurrent tumors in these patients were seeded by cells bearing ≥75% of the mutations detected in the initial tumors (as in patient 27, Fig. 1B). At the other end of the spectrum, tumors from three patients showed branched clonal evolution; we infer that the recurrent tumors in these patients were seeded by cells derived from the initial tumor at an early stage of its evolution, as the recurrent tumors shared ≤25% of mutations detected in the initial tumors. Patient 17 was an extreme example of branched clonal evolution, as the initial and recurrent tumors shared only the *IDH1* R132H ($Arg^{132} \rightarrow His$) mutation (Fig. 1C). This further implicates *IDH1* mutations as an initiating event in low-grade gliomagenesis (*12*). Indeed, *IDH1* mutation was the only shared mutation in every patient—an observation that supports the current interest in IDH1 as a therapeutic target (*16*). Paired tumors from the remaining 16 patients formed a continuum between linear and branched clonal evolution. Together, these data illustrate the extent to which genetically similar low-grade gliomas diverge after surgical resection, and suggest that recurrences may emerge from early stages in the evolution of the initial tumor.

Many solid tumors, including glioblastoma (GBM), display intratumoral heterogeneity (*17*, *18*). For example, geographically distinct parts of the tumor may have different mutations. Intratumoral heterogeneity could be a confounding factor in estimates of genetic divergence when only one relatively small fraction of a tumor is sampled. To explore the extent of intratumoral heterogeneity in our cases, we first analyzed the *BRAF* V600E ($Val^{600} \rightarrow Glu$) mutation that was subclonal in the initial tumor of patient 18 and undetectable in the recurrent tumor by either exome sequencing or droplet digital polymerase chain reaction (PCR) (Fig. 1D and fig. S3) (*10*). *BRAF* V600E was present in three of six additional samples from geographically distinct regions of the initial tumor, whereas seven additional samples of the recurrence all lacked this mutation. These results suggest that the *BRAF*-mutant clone did not expand, despite the proliferative advantage typically conferred by this mutation. Such a finding contrasts sharply with the selection and outgrowth of subclonal drivers during the evolution of chronic lymphocytic leukemias (*3*).

Beyond the actionable *BRAF* mutation, we sequenced the exomes of additional, geographically distinct samples from three cases to further determine the extent to which apparently private mutations might be misclassified because of intratumoral heterogeneity. In patient 17, for whom all mutations except *IDH1* were private, intratumoral heterogeneity was observed in the initial and recurrent tumor. From the mutational profiles, however, we inferred that three samples of the initial tumor and four samples of the recurrence all derived from a common tumor cell of origin that possessed only an *IDH1* R132H mutation (Fig. 2A and table S5). Moreover, the recurrent tumor contained driver mutations in *TP53* and *ATRX* distinct from those observed in the initial tumor. We found no evidence of these new *TP53* or *ATRX* mutations in the initial tumor at allele frequencies of ~0.1% (figs. S3 and S4), implying convergent phenotypic evolution (*5*) via a strong ongoing selection for loss of these genes. The initial and recurrent tumors likely did not arise independently, as they also shared three somatic noncoding mutations (fig. S5). Thus, the initial and recurrent tumors were only distantly related and, despite the local and relatively rapid recurrence (fig. S6), exonic mutations other than *IDH1* R132H were only transiently present during the course of this patient's disease. Finally, we sequenced the exomes of additional distinct samples of the initial and recurrent tumors from patients 26 and 27, broadening our assessment of the impact of intratumoral heterogeneity on the reported genetic divergence. We found that only a small minority of private mutations were actually shared events (7%; table S3) (*10*). Intratumoral heterogeneity therefore could not explain the majority of the genetic divergence between the initial and recurrent tumors in our cohort, including the driver mutations in initial tumors that were undetected in their recurrence.

To investigate whether sequential recurrences from a single patient could each be traced to the same evolutionary stage of the initial tumor, we sequenced the exomes of the second and third recurrent tumors from patient 04 and constructed a disease phylogeny by clonal ordering (Fig. 2B, fig. S7, and table S5) (*5*, *19*). The initial tumor and three sequential local recurrences were clonally related, as indicated by the shared phylogenetic branch containing early driver mutations in *IDH1* and *TP53*. We infer that the tumor cells seeding the second recurrence branched off from the initial tumor at a slightly earlier evolutionary stage than the cells seeding the first recurrence. In contrast, the third recurrent tumor was a direct outgrowth of the second recurrence. These results show that branched and linear patterns of clonal evolution occurred at differing times in the same patient and are therefore not intrinsic properties of the tumor.

Beyond maximal, safe, surgical resection, there is currently no standard of care for patients with low-grade glioma; options include surveillance, adjuvant radiation alone, TMZ alone, or radiation and TMZ. TMZ is an alkylating agent that induces apoptosis in glioma cells and is sometimes used to defer or delay the use of radiation. However, there is currently no information on whether treatment of grade II astrocytomas with TMZ confers longer overall survival (*8*). Because TMZ is also mutagenic (*20*), we sought to determine how adjuvant chemotherapy with TMZ affects the mutational profile of recurrent tumors by comparing the initial low-grade gliomas to their recurrence after treatment. Although the initial tumors and most of the recurrent tumors in our cohort had 0.2 to 4.5 mutations per megabase (Mb) (*21*, *22*), 6 of the 10 patients treated with

[1]Department of Neurological Surgery, University of California, San Francisco, CA 94158, USA. [2]Department of Pathology, University of California, San Francisco, CA 94158, USA. [3]Genome Science Laboratory, Research Center for Advanced Science and Technology, University of Tokyo, Meguro-ku, Tokyo 153-8904, Japan. [4]Department of Neurosurgery, University of Tokyo, Bunkyo-ku, Tokyo 113-8655, Japan. [5]Department of Medicine, University of California, San Francisco, CA 94158, USA. [6]Helen Diller Family Comprehensive Cancer Center, University of California, San Francisco, CA 94158, USA. [7]Department of Bioengineering and Therapeutic Sciences, University of California, San Francisco, CA 94158, USA. [8]Department of Radiology and Biomedical Imaging, University of California, San Francisco, CA 94158, USA. [9]Department of Pediatrics, University of California, San Francisco, CA 94158, USA. [10]Department of Neurology, University of California, San Francisco, CA 94158, USA. [11]Department of Epidemiology and Biostatistics, University of California, San Francisco, CA 94158, USA. [12]Institute for Human Genetics, University of California, San Francisco, CA 94158, USA. [13]Michael Smith Genome Sciences Centre, British Columbia Cancer Agency, Vancouver, BC V5Z 4E6, Canada.

*These authors contributed equally to this work.
†Present address: 23andMe Inc., Mountain View, CA 94043, USA.
‡Corresponding author. E-mail: jcostello@cc.ucsf.edu (J.F.C.); barry.taylor@ucsf.edu (B.S.T.)

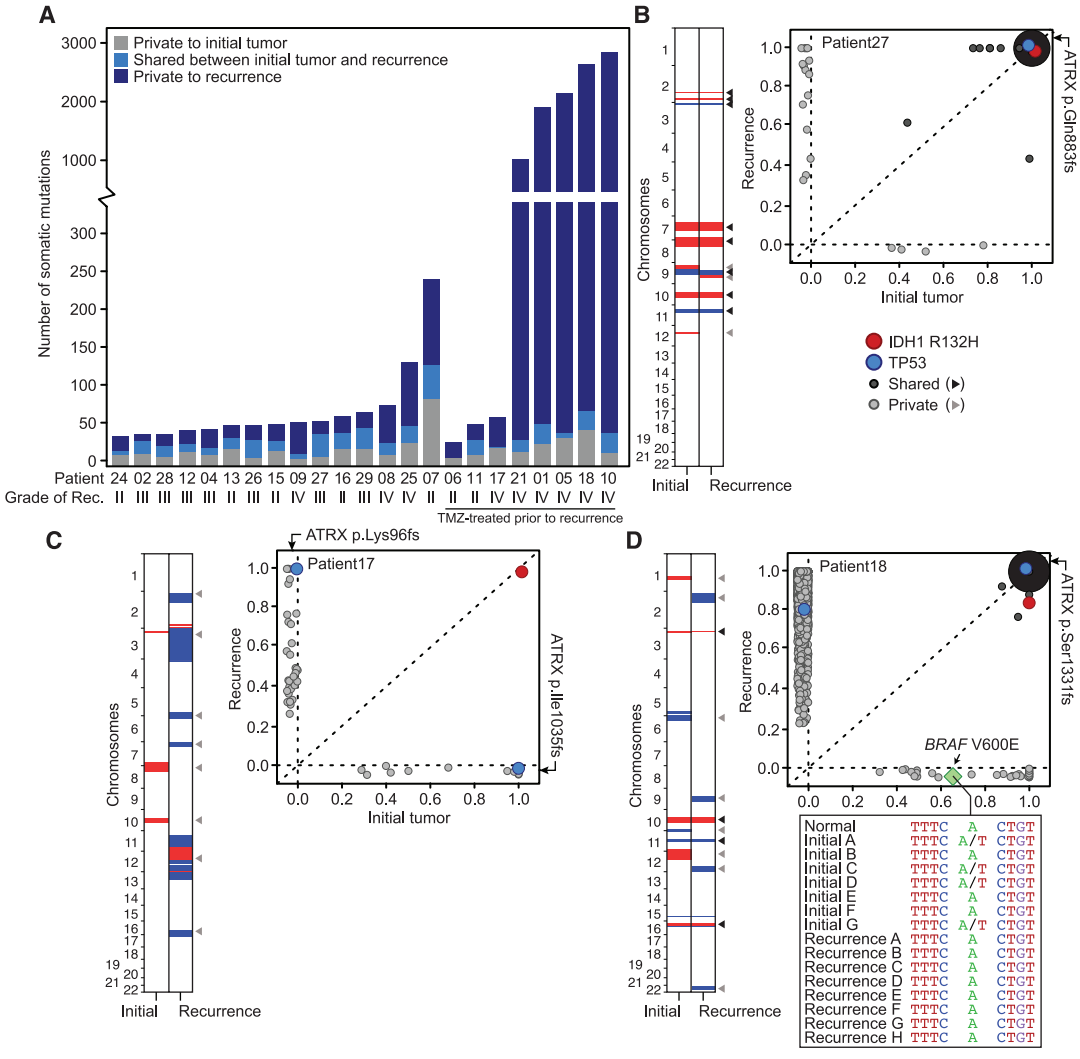

Fig. 1. Genetic landscapes of low-grade gliomas and their patient-matched recurrences. (**A**) Total number of mutations private to or shared between the initial and first recurrent glioma of 23 patients. (**B** to **D**) Shared and private somatic mutations in paired initial and recurrent tumors (*x* and *y* axes, respectively) as a function of the estimated fraction of tumor cells carrying the mutant allele. Mutations present in all the cells in both tumors are represented by a single point whose radius is scaled by the log count of such mutations. Shared and private CNAs are indicated (red and blue are gains and losses, respectively; white is copy-neutral). In (C), clonal *TP53* and *ATRX* mutations in the initial tumor were not identified in the recurrent tumor, but different clonal mutations in these two genes were acquired. (D) Inset shows the DNA sequence encompassing *BRAF* V600E in the normal tissue and in 15 geographically distinct samples of the initial and recurrent tumors.

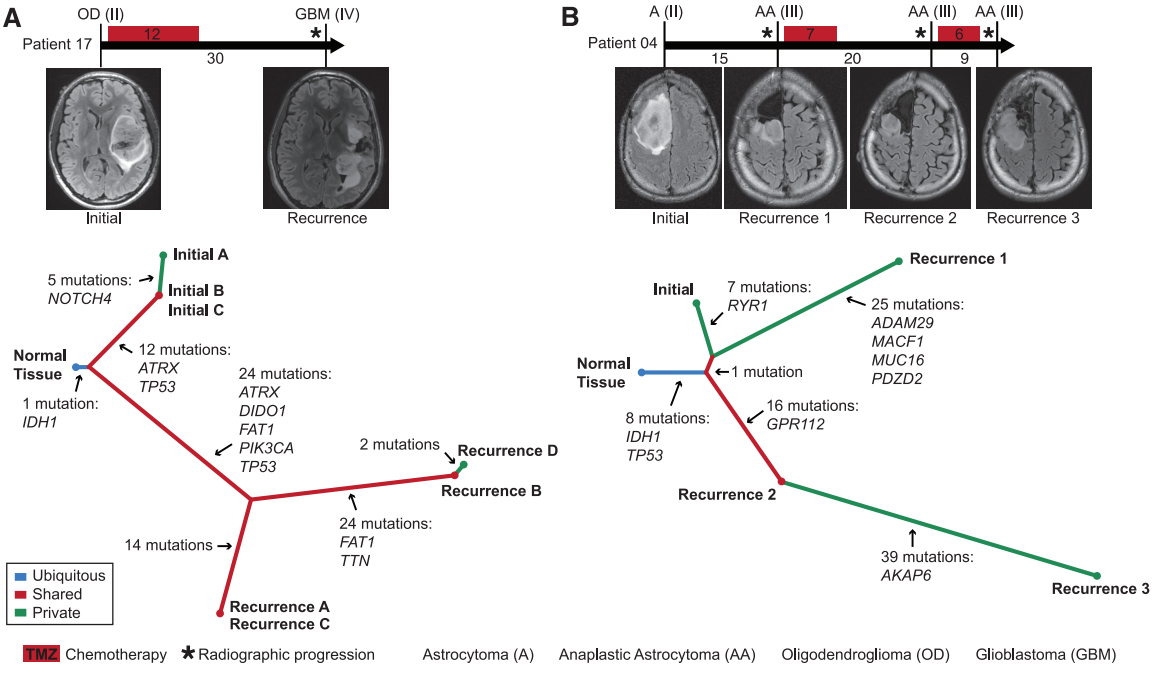

Fig. 2. Temporal and spatial patterns of clonal evolution in the tumors of two glioma patients. (**A** and **B**) A timeline of treatment histories for patient 17 (A) and patient 04 (B) (top, intervals labeled in months). Vertical bars correspond to the time of tumor resection and are labeled with the tumor diagnosis and grade. Representative MRIs are also shown. A phylogenetic tree (bottom) depicts the patterns of clonal evolution of these tumors inferred from the pattern and frequency of somatic mutations, highlighting genes frequently mutated in cancer.

TMZ had recurrent tumors that were hypermutated; that is, they harbored 31.9 to 90.9 mutations per Mb (table S6). Overall, 97% of these were C>T/G>A transitions predominantly occurring at CpC and CpT dinucleotides, which is a signature of TMZ-induced mutagenesis distinct from nonhypermutated tumors (fig. S8) (*20*, *22*, *23*). We classified C>T/G>A transitions in each hypermutated tumor as TMZ-associated if they were undetected in the matched initial tumor, which was resected before TMZ treatment (Fig. 3A). Although it is difficult to definitively attribute any single mutation to TMZ exposure, comparing the C>T/G>A mutation rates in each tumor pair suggested that >98.7% are due to TMZ-induced mutagenesis (*10*). To determine whether intratumoral heterogeneity in initial tumors resulted in the misclassification of some mutations as TMZ-associated, we sequenced the exomes of three additional geographically distinct samples of the untreated initial tumor from patient 18. For mutations classified as TMZ-associated, sequencing reads with the mutation were rare in the additional exomes and were found at rates no higher than expected by chance ($1.7 \pm 0.08\%$; $P = 0.5$, Wilcoxon rank-sum test) (*10*), further suggesting that they are induced by TMZ.

Resistance to TMZ develops in part through the acquisition of mutations that inactivate the DNA mismatch repair (MMR) pathway. MMR pathway dysfunction and continued TMZ exposure can in turn result in hypermutation (*22*–*25*). Indeed, we found that hypermutated tumors acquired somatic mutations in MMR genes that were not detected in their initial tumors, as well as aberrant DNA methylation of O^6-methylguanine-DNA methyltransferase (MGMT) (fig. S3, fig. S9, and table S1).

The introduction of thousands of de novo mutations may drive the evolution of TMZ-resistant glioma cells to higher states of malignant potential (*1*, *23*). Indeed, all six recurrent tumors that showed evidence of TMZ-induced hypermutation underwent malignant progression to GBM, a high-grade tumor with a worse prognosis (*8*, *9*). To investigate this hypothesis and to identify TMZ-associated mutations that may drive the outgrowth of GBM from low-grade glioma, we focused on the RB and Akt-mTOR signaling pathways, which are associated with high-grade gliomas (Fig. 3B) (*22*, *26*–*28*). In each hypermutated recurrence, TMZ-associated mutations affected genes coding for essential signaling molecules in these two pathways. For example, in the RB pathway we identified a TMZ-associated RB1 c.2520+1G>A splice-site mutation found previously in the germ line of patients with hereditary retinoblastoma (*29*, *30*). Transcriptome sequencing confirmed that this mutation triggered aberrant splicing, premature termination, and loss of the RB1 C-terminal domain necessary for growth suppression (Fig. 3C) (*31*). Recurrent tumors from patients 05 and 10 each had a TMZ-associated *CDKN2A* $Pro^{114} \rightarrow Leu$ mutation, which prevents $p16^{INK4A}$ protein encoded by this gene from inhibiting CDK4 or inducing cell cycle arrest (*32*). The same mutation has been reported in other tumor types (*33*) and in the germ line of patients with familial melanoma (*34*). Gene set enrichment analysis further confirmed the deregulation of RB1-mediated cell cycle control upon tumor recurrence (Fig. 3D), which suggests that TMZ-associated mutations compromise the function of the RB tumor suppressor pathway.

We also investigated TMZ-associated mutations that may activate the Akt-mTOR signaling pathway. We identified a TMZ-associated mutation (*PIK3CA* $Glu^{542} \rightarrow Lys$) in the recurrent tumor of patient 18 that drives Akt hyperactivation and induces mTOR-dependent oncogenic transformation (*35*). Similarly, the TMZ-treated second recurrence of patient 24 had TMZ-associated mutations in *PTEN* ($Ala^{121} \rightarrow Thr$ and $Gly^{165} \rightarrow Arg$) at residues critical to its phosphatase activity (*36*) that are recurrently mutated in GBM (*33*). Finally, we validated in vitro that a TMZ-associated *MTOR* S2215F ($Ser^{2215} \rightarrow Phe$) mutation in the recurrent tumor of patient 01 was constitutively

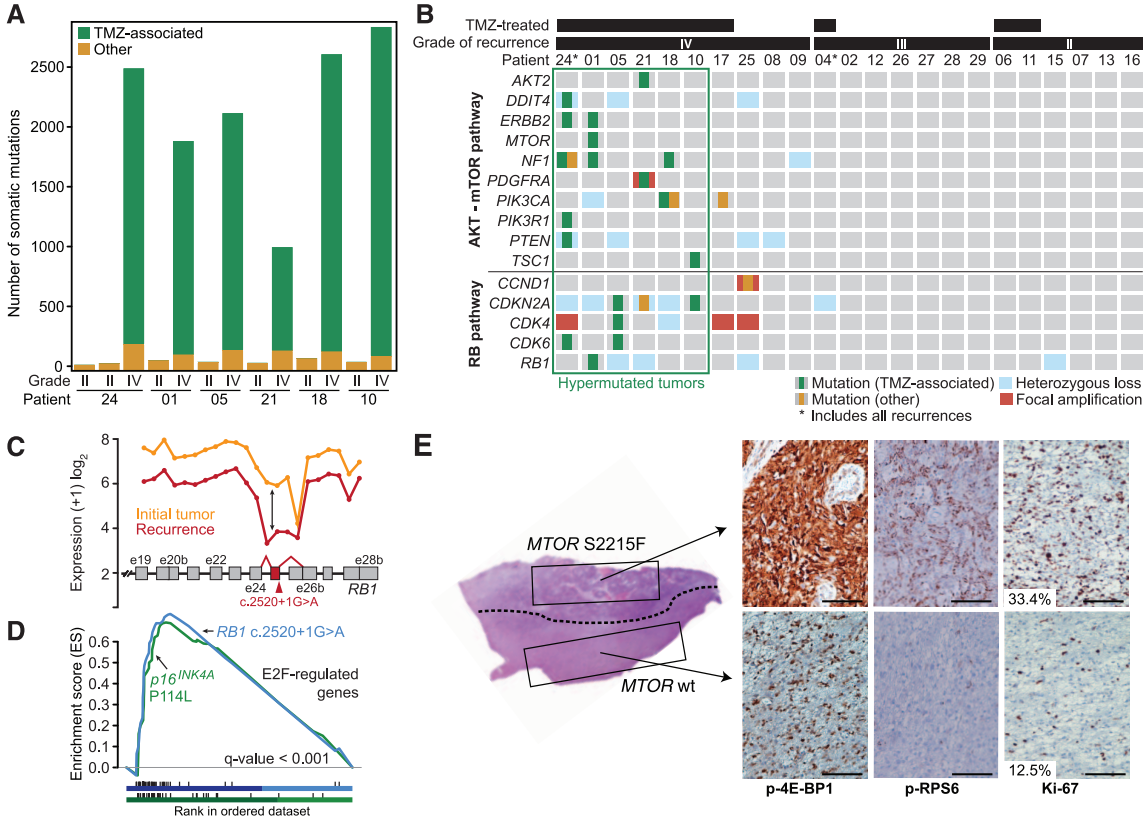

Fig. 3. Recurrent tumors from patients treated with TMZ harbor genetic alterations in the RB and Akt-mTOR signaling pathways. (**A**) Numbers of TMZ-associated mutations and other mutations identified in the six patients with hypermutated recurrent tumors. (**B**) Somatic mutations and CNAs acquired upon recurrence in key genes of pathways associated with GBM. (**C**) Expression level of *RB1* at each exon and exon-exon junction in the initial and recurrent tumor of patient 01 showing aberrant splicing of the *RB1* transcript in the recurrent tumor harboring the *RB1* c.2520+1G>A splice-site mutation. The *RB1* exon and exon junctions with significant differential usage (red) and the location of the splice-site mutation are shown. (**D**) Gene set enrichment analysis shows significant enrichment of genes down-regulated by *RB1* and up-regulated by *E2F* in the recurrent tumors of patients 01 (blue) and 10 (green), coincident with the acquisition of TMZ-associated mutations in the RB pathway. (**E**) Hematoxylin and eosin (H&E)–stained tumor sample from the first recurrent tumor of patient 01. A dotted line separates the two morphologically distinct regions. Immunohistochemistry (IHC) for phospho-RPS6, phospho-4E-BP1, and Ki-67 shows differential activation of mTORC1 targets and proliferation rates in the two adjacent regions. Scale bars, 100 μm.

activating (fig. S10), similar to the previously identified *MTOR* $Ser^{2215} \rightarrow Tyr$ (*37*). Moreover, adjacent regions of this recurrence showed heterogeneous mTOR complex 1 (mTORC1) activity (Fig. 3E and fig. S11). Microdissection revealed that although these adjacent regions shared a subset of the mutations found in the initial tumor, *MTOR* S2215F and other TMZ-associated mutations were present only in the region that stained strongly for mTORC1 activation, which also had higher staining of the proliferation marker Ki-67, implying that the TMZ-associated mutations conferred a proliferative advantage. A distal second recurrence harbored the same TMZ-associated mutations and stained strongly and homogeneously for mTORC1 targets (fig. S12). Although both regions of the first recurrence were GBM, the hypermutated subclone underwent in vivo selection, invaded distally, and seeded the second recurrence (figs. S13 and S14). Across our cohort, Akt-mTOR pathway mutations corresponded with elevated phospho-4E-BP1 and RPS6 in vivo, indicating hyperactivated mTORC1 in recurrent GBMs relative to their initial tumors (fig. S12).

There was no evidence that the mutations in the RB and Akt-mTOR signaling pathways preceded TMZ treatment, according to analysis of additional geographically distinct samples of initial tumors from four of the six patients with hypermutated recurrent tumors (table S7). Non-hypermutated recurrent tumors that progressed to GBM also acquired genetic changes in these signaling pathways, but through alternative mechanisms. In contrast, none of the grade II-III recurrences acquired mutations in these pathways. These data suggest a connection among TMZ treatment, driver mutations in oncogenic signaling pathways, and malignant progression.

Through direct comparison of the genomic landscape of gliomas at initial diagnosis and recurrence, we were able to infer the mutational character of the infiltrating tumor cells that give rise to recurrence and that adjuvant therapy with TMZ is intended to eliminate. Recurrences did not typically arise from cells bearing the full set of mutations found in the initial tumor, as would be expected from a local recurrence in the absence of selective pressure from adjuvant chemotherapy. This finding complicates the use of tumor genomics to design precision therapies targeting residual disease. We also demonstrated an alternative evolutionary path of low-grade glioma that is largely determined by adjuvant chemotherapy with TMZ. This extends earlier studies of primary GBMs (*23*, *25*), unpaired recurrent tumors (*22*), and a cell culture model (*20*). Future basic and clinical studies must weigh the initial antitumor effects of TMZ against the potential risk of inducing new driver mutations and malignant progression. Ultimately, a better understanding of the invading cells that give rise to recurrent tumors and the effect of adjuvant therapeutics on their evolution will facilitate the development of new strategies to delay or prevent recurrence and malignant progression.

References and Notes

1. M. Gerlinger, C. Swanton, *Br. J. Cancer* **103**, 1139–1143 (2010).
2. M. Greaves, C. C. Maley, *Nature* **481**, 306–313 (2012).
3. D. A. Landau *et al.*, *Cell* **152**, 714–726 (2013).
4. L. Ding *et al.*, *Nature* **481**, 506–510 (2012).
5. M. Gerlinger *et al.*, *N. Engl. J. Med.* **366**, 883–892 (2012).
6. S. Yachida *et al.*, *Nature* **467**, 1114–1117 (2010).
7. X. Wu *et al.*, *Nature* **482**, 529–533 (2012).
8. N. Sanai, S. Chang, M. S. Berger, *J. Neurosurg.* **115**, 948–965 (2011).
9. M. Westphal, K. Lamszus, *Nat. Rev. Neurosci.* **12**, 495–508 (2011).
10. See supplementary materials on *Science* Online.
11. Y. Jiao *et al.*, *Oncotarget* **3**, 709–722 (2012).
12. T. Watanabe, S. Nobusawa, P. Kleihues, H. Ohgaki, *Am. J. Pathol.* **174**, 1149–1153 (2009).
13. K. Watanabe *et al.*, *Clin. Cancer Res.* **3**, 523–530 (1997).
14. P. P. Medina *et al.*, *Hum. Mutat.* **29**, 617–622 (2008).
15. S. Glaros, G. M. Cirrincione, A. Palanca, D. Metzger, D. Reisman, *Cancer Res.* **68**, 3689–3696 (2008).
16. D. Rohle *et al.*, *Science* **340**, 626–630 (2013).
17. N. J. Szerlip *et al.*, *Proc. Natl. Acad. Sci. U.S.A.* **109**, 3041–3046 (2012).
18. A. Sottoriva *et al.*, *Proc. Natl. Acad. Sci. U.S.A.* **110**, 4009–4014 (2013).
19. L. M. F. Merlo, J. W. Pepper, B. J. Reid, C. C. Maley, *Nat. Rev. Cancer* **6**, 924–935 (2006).
20. W. J. Bodell, N. W. Gaikwad, D. Miller, M. S. Berger, *Cancer Epidemiol. Biomarkers Prev.* **12**, 545–551 (2003).
21. C. Greenman *et al.*, *Nature* **446**, 153–158 (2007).
22. Cancer Genome Atlas Research Network, *Nature* **455**, 1061–1068 (2008).
23. C. Hunter *et al.*, *Cancer Res.* **66**, 3987–3991 (2006).
24. D. P. Cahill *et al.*, *Clin. Cancer Res.* **13**, 2038–2045 (2007).
25. S. Yip *et al.*, *Clin. Cancer Res.* **15**, 4622–4629 (2009).
26. G. Reifenberger, J. Reifenberger, K. Ichimura, P. S. Meltzer, V. P. Collins, *Cancer Res.* **54**, 4299–4303 (1994).
27. H. Wang *et al.*, *Lab. Invest.* **84**, 941–951 (2004).
28. D. N. Louis, *Annu. Rev. Pathol.* **1**, 97–117 (2006).
29. T. Tsai *et al.*, *Arch. Ophthalmol.* **122**, 239–248 (2004).
30. C. Houdayer *et al.*, *Hum. Mutat.* **23**, 193–202 (2004).
31. X. Q. Qin, T. Chittenden, D. M. Livingston, W. G. Kaelin Jr., *Genes Dev.* **6**, 953–964 (1992).
32. J. Koh, G. H. Enders, B. D. Dynlacht, E. Harlow, *Nature* **375**, 506–510 (1995).
33. S. A. Forbes *et al.*, *Curr. Protoc. Hum. Genet.* Chapter 10, Unit 10.11 (2008).
34. M. C. Fargnoli *et al.*, *J. Invest. Dermatol.* **111**, 1202–1206 (1998).
35. S. Kang, A. G. Bader, P. K. Vogt, *Proc. Natl. Acad. Sci. U.S.A.* **102**, 802–807 (2005).
36. S. Y. Han *et al.*, *Cancer Res.* **60**, 3147–3151 (2000).
37. T. Sato, A. Nakashima, L. Guo, K. Coffman, F. Tamanoi, *Oncogene* **29**, 2746–2752 (2010).

Acknowledgments: We thank S. Gonzalez for assistance with the collection of clinical information; R. Kang for assistance with mutation validation; H. van Thuijl for assistance with MGMT methylation; and J. Wiencke and G. Hsuang for assistance with droplet digital PCR. Supported by Accelerate Brain Cancer Cure (J.F.C.), the Grove Foundation, the TDC Foundation, the Anne and Jason Farber Foundation, the Samuel Waxman Cancer Research Foundation, the Alex Lemonade Stand Foundation, the Entertainment Industry Foundation and Anne Feeley, and a generous gift from the Dabbiere family. Also supported by National Institute of General Medical Sciences grant T32GM008568 (T.M.); NIH grants 1T32CA15102201 and R25NS070680 (M.B.); NIH grant P50CA097257 (L.E.J., S.J.N., M.S.B., S.M.C., J.F.C., and B.S.T.); National Cancer Institute grants R01CA169316-01 (J.F.C.), P01CA81403 (W.C.G., E.C., and W.A.W.), P30CA82103 (A.B.O.), and R01CA163336 (J.S.S.); National Institute of Neurological Disorders and Stroke grant K08NS079485 (W.C.G., E.C., and W.A.W.); the UCSF Academic Senate and the Sontag Foundation (J.S.S., J.F.C., and B.S.T.); the BC Cancer Foundation, Genome BC, and Genome Canada (M.A.M.); the Goldhirsh Foundation (J.F.C.); and a research program of the Project for Development of Innovative Research on Cancer Therapeutics (P-Direct) (A.M., N.S., and H.A.), Grant-in-Aid for Scientific Research on Innovative Areas (no. 23134501) (A.M.), and Grant-in-Aid for Scientific Research (S) (no. 24221011) (H.A.) from the Ministry of Education, Culture, Sports, Science and Technology of Japan. C.Y.M. was a Damon Runyon Cancer Research Postdoctoral Fellow. M.A.M. is a Canada Research Chair in Genome Science. All exome and transcriptome sequencing data have been deposited in the European Genome-phenome Archive under accession number EGAS00001000579, and data from patients 24 to 29 have also been deposited to the Japanese Genotype-phenotype Archive under accession number JGAS00000000004.

Supplementary Materials

www.sciencemag.org/content/343/6167/189/suppl/DC1
Materials and Methods
Figs. S1 to S14
Tables S1 to S7
References (*38*–*61*)

2 May 2013; accepted 27 November 2013
Published online 12 December 2013;
10.1126/science.1239947

Single-Cell RNA-Seq Reveals Dynamic, Random Monoallelic Gene Expression in Mammalian Cells

Qiaolin Deng,[1]* Daniel Ramsköld,[1,2]* Björn Reinius,[1,2] Rickard Sandberg[1,2]†

Expression from both alleles is generally observed in analyses of diploid cell populations, but studies addressing allelic expression patterns genome-wide in single cells are lacking. Here, we present global analyses of allelic expression across individual cells of mouse preimplantation embryos of mixed background (CAST/Ei × C57BL/6J). We discovered abundant (12 to 24%) monoallelic expression of autosomal genes and that expression of the two alleles occurs independently. The monoallelic expression appeared random and dynamic because there was considerable variation among closely related embryonic cells. Similar patterns of monoallelic expression were observed in mature cells. Our allelic expression analysis also demonstrates the de novo inactivation of the paternal X chromosome. We conclude that independent and stochastic allelic transcription generates abundant random monoallelic expression in the mammalian cell.

In diploid organisms, the zygote inherits one set of autosomal chromosomes from each parent. Although it is widely believed that transcription of autosomal genes occurs from both parental alleles, specific classes of genes have been shown to express only one, randomly